applied sciences

MDPI

Article

Ammonia Gas Adsorption in Fixed Bed and Fluidized Bed Using Bentonite Particles

Gabriela Muntianu [1,*], Ana-Maria Georgescu [1], Ana-Maria Rosu [1,*], Nicoleta Platon [1], Vasilica Alisa Arus [1], Cosmin Valeriu Jinescu [2] and Ileana Denisa Nistor [1]

[1] Department of Chemical and Food Engineering, "Vasile Alecsandri" University of Bacau, 157 Calea Mărăsesti Street, 600115 Bacau, Romania; ana.georgescu@ub.ro (A.-M.G.); nicoleta.platon@ub.ro (N.P.); morarescua@ub.ro (V.A.A.); dnistor@ub.ro (I.D.N.)

[2] Department of Industrial Process Equipment, Politehnica University of Bucharest, 313 Splaiul Independentei Street, 060042 Bucharest, Romania; cosmin.jinescu@yahoo.com

* Correspondence: muntianu.gabriela@ub.ro (G.M.); ana.rosu@ub.ro (A.-M.R.)

Abstract: The present paper investigates the ammonia adsorption kinetic from air on sodium bentonite particles and on aluminum pillared bentonite particles in fixed bed and fluidized bed. The sodium bentonite is used as adsorbents and as raw material for chemically modified bentonite with aluminum polyhydroxocations. The aluminum pillared bentonite is prepared by a classical pillaring process to create high porosity and to increase the ammonia particle surface contact. Adsorbents used were characterized by the following analysis: granulometric distribution, acid–base character determination by Thermal Programmed Desorption (TPD), elemental microanalysis by Energy Dispersive X-Ray coupled with scanning electron microscopy (EDX-SEM), X-Ray diffractograms, adsorption–desorption isotherms by Brunauer–Emmett–Teller method and distribution of pore sizes and pore volume calculation by Barrett–Joyner–Halenda method. The variable parameters used in ammonia adsorption capacity on bentonite particle determination are particles size, gas velocity and total gas flow rate. The parameters kept constant during the ammonia adsorption process on bentonite particles are geometric ratio, adsorbent mass and initial ammonia gas concentration. The ammonia adsorption capacity on sodium bentonite particles and on aluminum pillared bentonite particles was measured until bed saturation as a function of the gas–particle contact technique. The best results are obtained with homogeneous fluidization with small gas bubbles for the aluminum pillared bentonite particles after 100 s bed saturation with ammonia adsorption capacity of 0.945 mmol NH_3/g. To complete the study, ammonia desorption determination was carried out by a thermo-desorption process in order to recover the used particles. The adsorbent particles studied proved to be high-performance materials in order to use them in ammonia air depollution. Fluidized bed adsorption can be an efficient technique to accelerate mass transfer between ammonia from air and adsorbent particles.

Keywords: ammonia adsorption; sodium bentonite; aluminum pillared bentonite; fixed bed; fluidized bed; particle regeneration

check for updates

Academic Editor: Juan García Rodríguez

Received: 23 November 2024
Revised: 13 January 2025
Accepted: 14 January 2025
Published: 16 January 2025

Citation: Muntianu, G.; Georgescu, A.-M.; Rosu, A.-M.; Platon, N.; Arus, V.A.; Jinescu, C.V.; Nistor, I.D. Ammonia Gas Adsorption in Fixed Bed and Fluidized Bed Using Bentonite Particles. *Appl. Sci.* **2025**, *15*, 832. https://doi.org/10.3390/app15020832

Copyright: © 2025 by the authors. Licensee MDPI, Basel, Switzerland. This article is an open access article distributed under the terms and conditions of the Creative Commons Attribution (CC BY) license (https://creativecommons.org/licenses/by/4.0/).

1. Introduction

Intense industrial activities are one of the most important current problems because large quantities of pollutants, coming from different sources, are generated in the atmosphere with a direct influence on environmental degradation and the population's health. One of the strategies in environmental protection consists of developing some adsorbent

materials that allow the retention of such toxic gases before releasing them into the atmosphere [1]. High levels of harmful gases are present in the environmental medium from chemical factories such as carbon monoxide, hydrogen chloride, chlorine, hydrogen sulfide, nitrogen oxide, ozone, ammonia, etc. [2,3].

Ammonia is a relatively strong base and the most useful chemical in modern society. It can be used as a fertilizer (anhydrous ammonia, aqua ammonia and urea), as a precursor to nitrogenous compounds, as a cleaner, in plastic products, fuels, explosive production, etc. [4]. A large amount of ammonia has increased dramatically in the atmosphere due to these industrial exhaust emissions from livestock farming as domestic pollutants and from agriculture [5,6].

Ammonia is a very toxic, corrosive, flammable and explosive substance under certain conditions. Ammonia gas produces undesirable odors, which cause, in humans, severe burning of the eyes, skin and respiratory irritation at a concentration as low as 50–100 ppm [7], and at higher quantities, death is induced in a few minutes [7,8].

Adsorption is one of the techniques that can be used to capture ammonia gas and to control the concentration in the released gas flow [2]. Various adsorbents were developed for environmental remediation, including carbon-based adsorbent (lignite, biochar, activated carbon [8] and resin), metal–organic framework, mineral clays (bentonite, zeolite) and their modified forms (nanomaterials) [9].

In terms of the structural properties, adsorptive characteristics and environmental applications, bentonite and their derivatives [10–12] may be good candidates regarding gas–particle contact and to solve the problem of controlling the ammonia concentration in air [13].

Bentonites are mineral clays that are found in nature with no toxic effects on ecosystems and a low price of purification. These are components of soils, valuable in many branches of industries at the local level (chemicals, food processing, construction, pharmaceutical and cosmetic products, ceramics, etc.) [14], composed more precisely of at least 50% montmorillonite, a phyllosilicate of the smectites family. This smectite family consists of a 2:1 layer phyllosilicate constituted by an octahedral sheet containing Al^{3+}, Mg^{2+} or $Fe^{2+/3+}$ ions between two tetrahedral silica sheets [1,15], which shows the ability to swell by incorporating water or other molecules in the interlayer regions, like ammonia molecules [16].

Sodium bentonite in its natural or chemically modified state is used in this research as an adsorbent because it has the following properties: adsorption and ion exchange capacity [17–20], wide surface area and permanent porosity [21], acid–base character [12–26], and regeneration capacity after repeated adsorption processes [17].

Aluminum pillared bentonite is the modified adsorbent used for ammonia adsorption in different methods of gas–particle contact. This material was made in the laboratory by the pillaring method with the following steps: bentonite hydration and pillaring agent preparation by hydrolysis, bentonite suspension intercalation with the pillaring agent that contains aluminum polyhydroxocations [27–29], repeated washings and filtration, drying, calcination [30–33], and trituration in small particles.

However, gas–particle contact [34] involving sodium bentonite and aluminum pillared bentonite as adsorbents for ammonia adsorption capacity determination presents a major challenge in a static regime (in fixed bed or expanded bed) and in a dynamic regime (fluidized bed).

The fixed bed is formed at low gas velocities when the particles move separately, a certain vibration of them appears and the bed becomes expanded. The ammonia gas flows between particles, and the gas–particle surface contact is minimal. The fixed bed operation is carried out at $U_g < U_{mf}$.

In a fixed bed, variation of ammonia adsorption capacity depending on gas–particle contact is produced due to the mass transfer zone that moves from the inlet to the outlet of the adsorption column while the particle bed saturates [35]. In many fixed bed configurations, the adsorption process is limited by the transport of molecule gas into the interior of the particles [36]. In a fixed bed, the mass transfer is carried out by molecular diffusion, and in a fluidized bed, it occurs as an effect of the particle movement mainly by molecular diffusion and by convective diffusion [37].

The main objective of this paper on adsorption in a fluidized bed is to provide additional energy cost to overcome the inter-particle forces that are responsible for the cohesion of the small particles and other non-homogeneities during fluidization, like bubbling or slugging. Knowledge of dynamic conditions is essential for a good implementation of a fluidized bed in the retention of ammonia on bentonite particles [38,39].

The aim of this study is to compare the ammonia adsorption kinetics in fixed and fluidized beds depending on the surface contact between the gas and bentonite particles. The low economic cost is given by the use of a low flow rate at the minimum fluidization velocity.

An innovative objective in this research is testing, for the first time, new materials, such as as clay minerals, obtained by pillaring with aluminum polyhydroxocations during ammonia adsorption. In the literature, the adsorption of this pollutant in the liquid medium has been studied [40], and the novelty of this research is the adsorption of ammonia from the air by using fluidization as the gas pillared bentonite particle contact method.

The research ends with the study of the regeneration cycles of the adsorbent particles by thermo-desorption. The effect of the temperature is very important if the ammonia desorption is by chemisorption [41–43] between the particles and gas molecules. In such cases, an increase in the temperature up to 300 °C can favor the desorption of ammonia gas from the bentonite particles [44]. One of the essential conditions for an efficient adsorbent is that it can be easily recovered and the thermo-desorption process should be as economical possible.

2. Materials and Methods

2.1. Materials and Reagents for Pillaring Process

The raw material used for aluminum pillared bentonite was sodium bentonite ($Al_2H_2Na_2O_{13}Si_4$), supplied by Merck Romania SRL, an affiliate of Merck KGaA, Darmstadt, Germany. According to the supplier, the mineral composition for sodium bentonite is 99% montmorillonite, 0.05% cristobalite, 0.05% quartz and impurities [42]. The aluminum pillared bentonite is obtained using as reagents hexahydrate aluminum chloride (provide by Lachner, Neratovice, Czech Republic) and sodium hydroxide (provide by Chemical Company, Iasi, Romania).

2.2. Preparation Method of Aluminum Pillared Bentonite

A known concentration of sodium hydroxide solution of 0.2 mol/L was slowly added to a hexahydrate aluminum chloride solution of 0.2 mol/L in order to maintain a constant molar ratio of OH^-/Al^{3+} at 2.2. During the addition, the temperature was kept constant at 30 °C and the obtained solution was vigorous stirred to prevent local accumulation of hydroxyl ions that can produce precipitation of aluminum hydroxyls. This solution represents the pillaring agent. It contains polyhydroxocations of aluminum and is aged for 48 h and stored in a dark place at ambient temperature. The pillaring agent was incorporated by dropwise addition to 2 wt. % of sodium bentonite suspension under continuous stirring at constant temperature. The amount of aluminum cations per gram of bentonite is 10 mmol Al^{3+}/g. The sample was aged for 48 h in a dark place at ambient

temperature. After aging, the intercalated bentonite with aluminum polyhydroxocations was washed with deionized water repeatedly until chloride ions were removed (negative silver nitrate test). The freshly washed aluminum pillared bentonite samples were dried in an oven Air Performance AP60 (Precisa, Sibiu, Romania) at 120 °C for 4 h. The sample was subsequently calcined in an oven Caloris L 1003 (Caloris Group, Bucharest, Romania) at 400 °C for 2 h at a heating rate of 2 °C/min, then manually triturated, and sieved in two particles sizes with an average diameter ($\overline{d}_p$) of 750 μm and 1500 μm.

2.3. Preparation of Adsorbent Particles

The sodium bentonite was supplied as a powder and, to obtain particles, was agglomerated at a ratio of (1:3) with deionized water and dried in an oven ProLabo at 110 °C for 36 h.

The sodium bentonite and the aluminum pillared bentonite used were triturated and sieved with a Vibratory Sieve, series AS 200 (Retsh GmbH, Haan, Germany) by vibration at a speed of 700 rpm for 10 min. Three particle size classes were determined: $\overline{d}_p = 1500$ μm, $\overline{d}_p = 750$ μm and $\overline{d}_p = 350$ μm. The first two particle size classes were used as adsorbent particles, and the last particle size class of fine particles were used in characterization techniques.

The adsorbent particles were dried at 110 °C for 24 h and finally cooled at ambient temperature in a glass desiccator to ensure identical initial conditions for all adsorption tests.

2.4. Equipment for Adsorbent Characterization

The Ankersmid Eyetech particle characterization analyzer was used for particle size determination. The measuring range of this device is 0.1–300 μm by immersing the sample in water at 3 mg/mL concentration, at 23 °C. The optocoupler frequency was 200 Hz and the rotation speed was 12,000 rpm.

Thermal Programmed Desorption (TPD) measurements were achieved using ammonia and carbon dioxide as sample gases and are supposed to be quite representative for investigating the interactions occurring between gases and adsorbent surfaces.

Determination of acid–base character was realized in an installation including a cylindrical glass micro-reactor (2 mm internal diameter) with interior filaments that allow bentonite sample heating according to software. The gas carrier is dry nitrogen at normal pressure. In this device, a maximum of 200 mg of calcined bentonite powder under a controlled temperature (500 °C) was introduced to obtain a 2–3 cm height fixed adsorbent bed. In order to determine the surface acidity of the adsorbent, the ammonia gas was injected in fixed clay bed at 150 °C in ascending mode to 500 °C.

Ammonia or carbon dioxide gases were injected through the fixed clay bed until saturation, and the excess of the molecule gas was purged at the respective temperature in a vessel with water. After the removal of the two gases, in the installation, the nitrogen gas continued to flow in order to remove the traces of ammonia gas or carbon dioxide that were not adsorbed physically or chemically on sodium bentonite. The desorption was realized by heating the sodium bentonite at 500 °C. The desorbed gas was bubbled in a titration device previously prepared, containing sulfuric acid solution or sodium hydroxide solution in the presence of Tashiro indicator. The excess gas was volumetrically titrated.

Through TPD analysis, the distribution of acidic sites or basic sites and calculation of surface acidity or basicity limited by the TPD curve can be determined.

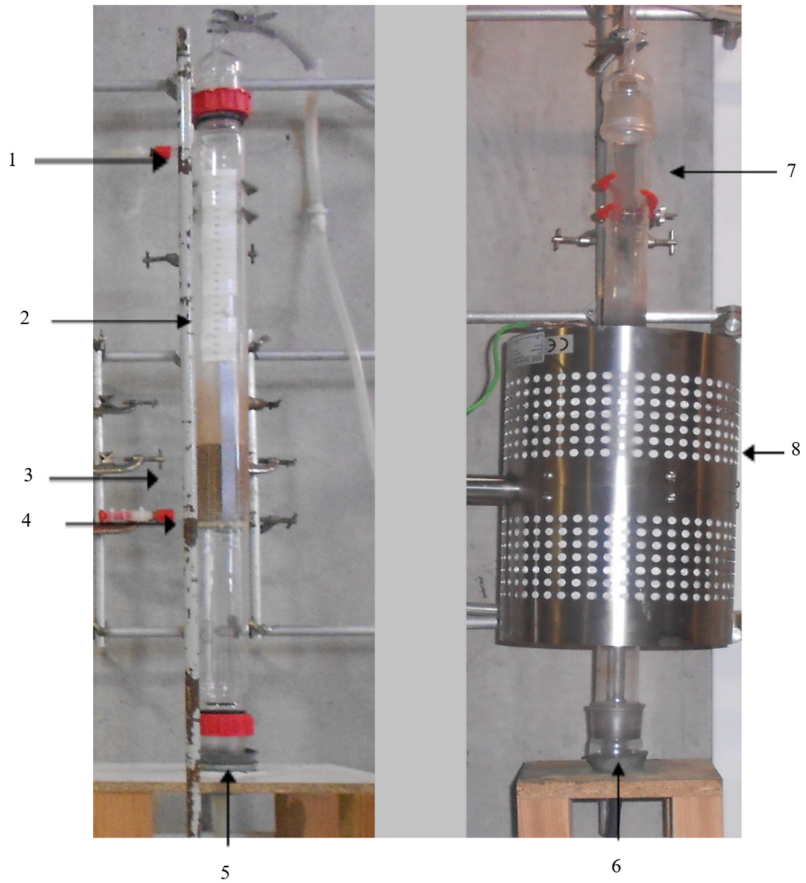
X-Ray Diffraction (XRD) analysis on a Siemens/Bruker D5000 X-Ray Powder Diffraction (XRD) System using CuKα radiation at λ = 1.5406 Å was carried out to obtain the specific X-Ray diffractograms and for basal spacing (d_{001}) calculation for the materials used as absorbents.

To complete the sample characterization, the Brunauer–Emmett–Teller (BET) method for specific surface area analysis and Barrett–Joyner–Halenda (BJH) method for distribution of pore sizes and pore volume calculation were applied using a Beckman Coulter SA 3100 equipment. Prior to the nitrogen adsorption–desorption measurements, the samples were degassed at 120 °C for 12 h.

Energy Dispersive X-Ray (EDX) analysis, carried out concomitantly with SEM microscopy, was performed for elemental microanalysis on a certain surface of sodium bentonite and aluminum pillared bentonite using an EDX ZAF Quantification.

2.5. Ammonia Adsorption and Desorption Procedure

The study of ammonia adsorption isotherms and kinetics in a fixed bed [35] and in a fluidized bed [33] on sodium bentonite particles and aluminum pillared bentonite particles has been carried out in an experimental installation shown in Figure 1a. After the adsorption process, the materials were subjected to the desorption of ammonia molecules from the particles with the help of nitrogen vapors by thermo-desorption. The particles saturated in ammonia were found in the column in a fixed bed to verify the recycling possibility and regeneration without major structural damage. The experimental thermo-desorption installation is shown in Figure 1b.



(**a**) *Ammonia adsorption* (**b**) *Ammonia thermo-desorption*

Figure 1. Experimental installations. 1—adsorption column; 2—graduated scale; 3—particle bed; 4—porous support; 5—mixed ammonia and air; 6—nitrogen gas; 7—desorption column; 8—electrical resistance.

The experimental installations used for ammonia adsorption–desorption are composed of a Pyrex transparent column with internal diameter of 5×10^{-2} m provided with a graduated scale for measuring the particle bed height. On the inlet of the mixed gases, a

porous plate can be found with pore size diameter of 60–100 μm for the uniform distribution of gases, which plays a supporting role for the particle bed. At the top of the column, a filter is placed with a pore size diameter of 0.44 μm to avoid fine particle transport during fluidization.

The adsorption installation, as shown in Figure 1a, is equipped with three gas routes, one for ammonia gas with 99.95 purity grade, one for compressed air and the last route for gases mixing (ammonia and air). Two gases passed separately through two Brooks Sho-Rate flow meters: one for ammonia gas from the bottle with flow range from 0 to 2.5 L/min and another for compressed air with flow range from 0 to 60 L/min, which passes through a granular drierite column to absorb the humidity from the air. The gases meet in a mixing system to obtain the known initial ammonia concentration (C_0) before starting the adsorption tests. Concentrations are expressed in parts per million (ppm).

Ammonia adsorption capacity was measured until saturation of the bed particles on inlet/outlet of the adsorption column using an Agilent Technologies 3000A 4-Channel Micro GC G2802A, Markham, ON, Canada. The non-adsorbed ammonia was removed and neutralized into a gas scrubber that contained an acid solution and the saturated particles were placed in the desorption installation for regeneration.

Ammonia test results were determined by reference to the calibration curve made before starting the adsorption experiments. Adsorption ammonia capacity in a fixed bed and fluidized bed under saturation conditions was calculated using specific equations [17,35,44] and expressed in mmol NH_3/g of bentonite. The variable parameters for testing the ammonia adsorption capacity are average particle diameter, $\overline{d}_p$, gas velocity, U_g, and total gas flow (ammonia and air), Q_T.

The parameters kept constant during the adsorption tests and their approximate values are adsorbent mass at 200 g, geometric ratio (L_0/D) at 2 and initial ammonia concentration at 3800 ppm. All ammonia adsorption experiments were carried out at ambient temperature in different gas–particle contact conditions: in a fixed bed or packed bed, under incipient fluidization and homogeneous fluidization with small gas bubbles in the bed.

The desorption installation is composed of a Pyrex transparent column with an internal diameter of 3.5×10^{-2} m, a porous support, one trace for nitrogen gas and cylindrical electrical resistance for heading the particle bed, as presented in Figure 1b.

The experimental parameters in ammonia desorption tests are the following: bed particles height: 1, heating temperature: 300 °C, time contact: 2 h and the dry nitrogen flow: 0.1 L/min.

Ammonia molecules desorbed from the particle bed were neutralized by the acidic solution under magnetic stirring at 200 rpm to cool the vapors until the pH value was 10. Calculation of the ammonia thermo-desorption capacity was performed using the Hendenson–Hasselbalch equation (Equation (1)) involving the pH determination for weak acid and pKa for ammonia ion, with a value of $\left[NH_4^+\right]$~9.25.

$$pH = pK_a + \log \frac{[NH_3]}{NH_4^+} \quad (1)$$

The ammonia solution is passed into the wastewater collector. This procedure was repeated using the same initial ammonia concentration of 0.0034 L/L until particle saturation and ammonia thermo-desorption capacity was measured using the same device as in the case of ammonia adsorption capacity determination.

3. Results and Discussion

3.1. Sodium Bentonite Characterization

3.1.1. Granulometric Distribution

The granulometric distribution for sodium bentonite was obtained for fine particles. The particle size distribution for sodium bentonite was obtained for particles that pass through the sieve (undersize) and for particles that remain on the sieve (oversize). Table 1 presents the mean diameter values for the sodium bentonite depending on length, length weighted, surface, surface weighted, volume and volume weighted. It can be observed that the mean diameter depending on the length, D[1,0], shows a particle size of 11.74 µm (this value represents the frequently encountered, average size); the standard deviation (STD) has a value of 1.40 µm and the confidence level (Conf.) is 98.11%.

Table 1. Statistical data obtained from the granulometric distribution for sodium bentonite.

Mean Diameter by:	Size (µm)	STD (µm)	Conf. (%)	Dimension	D10 (µm)	D50 (µm)	D90 (µm)	Mode (µm)
Length, D[1,0]	11.74	1.40	98.11	Number	10.30	11.49	13.87	10.30
Length weighted, D[2,1]	11.91	1.47	98.10	Length	10.30	11.49	13.87	10.30
Surface, D[2,0]	11.83	-	-	-	-	-	-	-
Surface weighted, D[3,2]	12.09	1.52	47.43	Surface	10.30	12.08	13.87	10.30
Volume, D[3,0]	11.91	-	-	-	-	-	-	-
Volume weighted, D[4,3]	12.28	1.57	47.41	Volume	10.30	12.08	14.46	10.30

Percentiles like D10, D50 and D90 can be obtained directly from Table 1 depending on the number of particles, length, surface and volume. The granulometric distribution on sodium bentonite by volume presents values for percentile D10; 10% of the number of particles (100%) have particle size under 10.30 µm; for percentile D50, 50% of the number of particles (100%) have particle size under 12.08 µm; for percentile D90, 90% of the number of particles (100%) have particle size under 14.46 µm.

Figure 2 shows the volume histogram and cumulative oversize for sodium bentonite with a mean diameter of 12.28 µm, standard deviation (STD) of 1.57 µm and confidence level (Conf.) of 47.41%.

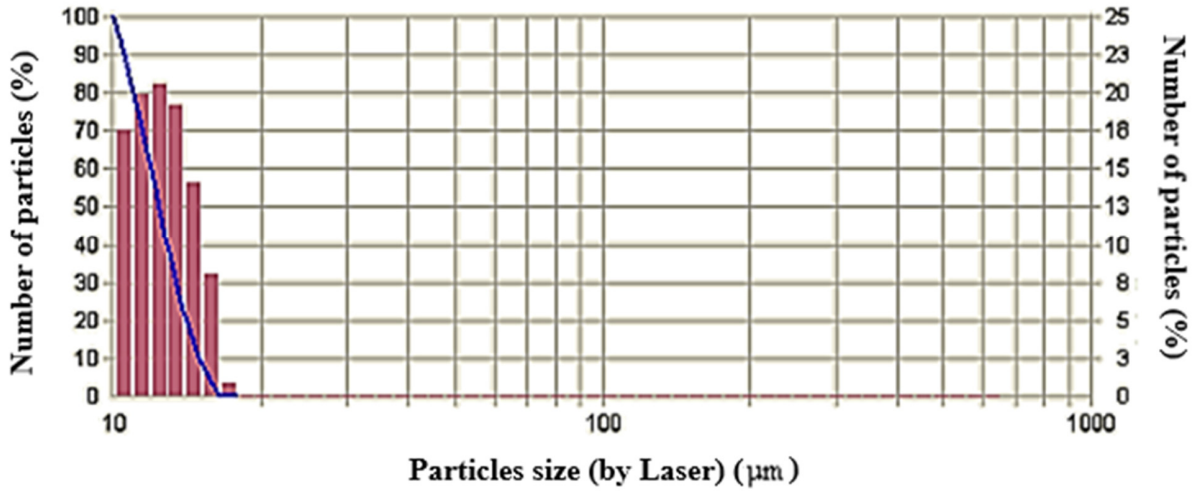
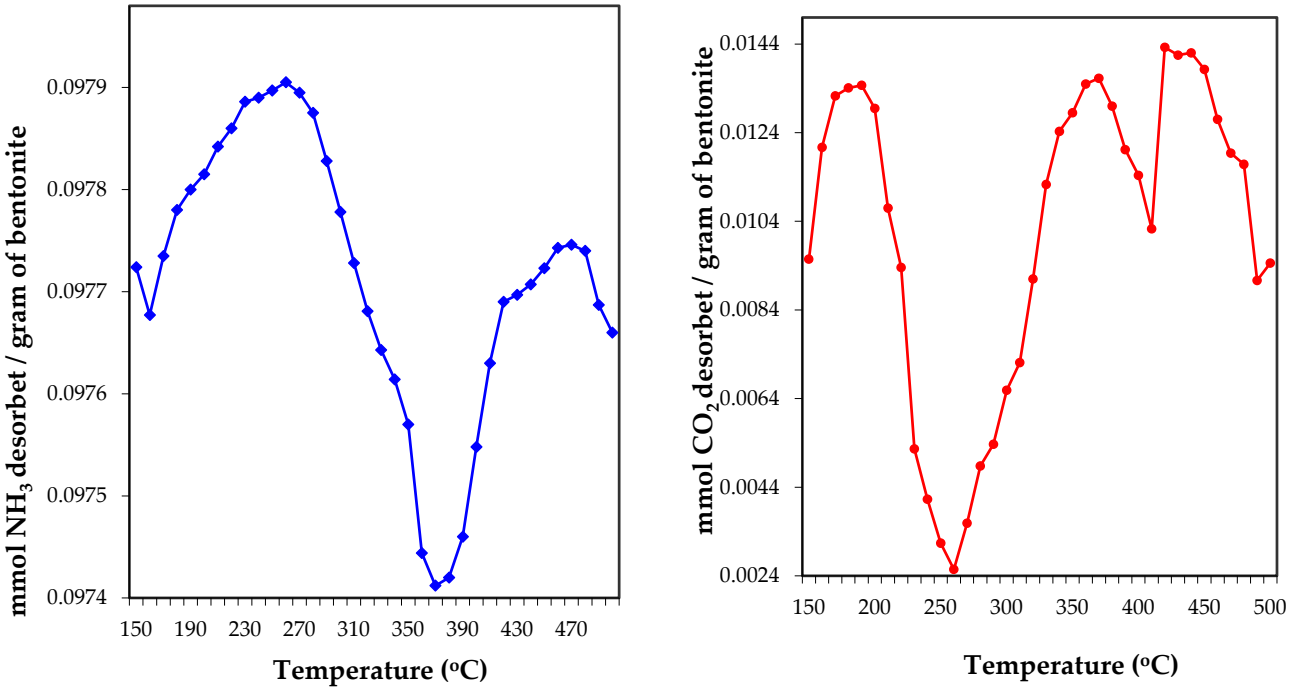


Figure 2. Volume histogram and cumulative oversize of sodium bentonite with D10: 10.30 µm; D50: 12.08 µm; D90: 14.46 µm.

Figure 2 presents a single granulometric distribution class that corresponds to the range of 10–28 μm with 0–82%. The particle size taken in the analysis of the sodium bentonite (raw material for aluminum pillared bentonite) is 12.08 μm and can be easily agglomerated with water to form particles of larger diameters.

3.1.2. Measurement of Surface Acidity and Surface Basicity

In order to establish the acid–base character on sodium bentonite, a series of experiments were carried out, measuring the surface acidity and surface basicity. The dependence of ammonia concentration and carbon dioxide concentration expressed in terms of mmol of desorbed gas/g of dry bentonite and the variation of temperature are shown in Figure 3. The thermal program is set to heating the sample in the range of 150–500 °C.



(**a**) (**b**)

Figure 3. Distribution of the acidic sites/basic sites of sodium bentonite. (**a**) NH_3-TPD curve; (**b**) CO_2-TPD curve.

The NH_3-TPD curve for sodium bentonite shows the existence of acidic sites present on the clay surface. It can be divided into acidic sites of medium strength with desorption temperature of 370 °C, representing 72.91% of the surface acidity, and acidic sites with high strength that are desorbed if they are subjected to a higher desorption energy, manifested by an increase in temperature from 370 to 450 °C, representing 27.08% of the surface acidity. The total surface acidity is 3.6153 mmol NH_3 desorbed/g of bentonite.

Analyzing the CO_2-TPD curve for sodium bentonite, it can be observed that the basic sites are divided into two domains. The first range is between 80 and 260 °C and corresponds to the desorption of carbon dioxide on basic sites, representing 28.17% of the surface basicity. The second temperature range (260–400 °C) represents 71.82% of surface basicity. The total basicity is 0.1471 mmol desorbed CO_2/g of bentonite.

3.2. Aluminum Pillared Bentonite Characterization

3.2.1. X-Ray Diffraction (XRD)

In order to verify the successful pillaring process of sodium bentonite, XRD measurements were carried out. The intercalation of sodium bentonite with aluminum polyhydroxocations determined the modification of basal spacing (d_{001}). Figure 4 presents the XRD diffractogram for the two adsorbents studied. The position of the d_{001} peak, which allows us to determine the basal spacing, was shifted to a lower value of 2 theta angle.

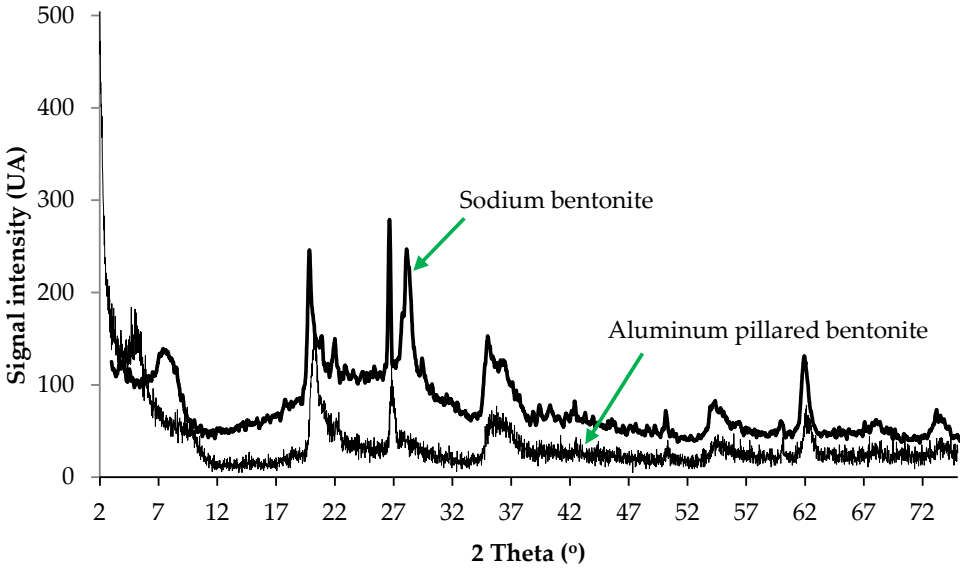


Figure 4. X-Ray diffractograms and the basal spacing of the adsorbents.

The values of basal spacing are very important, because they give clear information concerning the pillaring process. The basal spacing has increased from 11.66 Å for sodium bentonite to 18.78 Å for aluminum pillared bentonite. The aluminum pillared bentonite obtained after pillaring must have an accessible porosity for retaining gas molecules and providing thermal resistance for the desorption and regeneration of material.

3.2.2. Nitrogen Adsorption–Desorption

Figure 5 represents the nitrogen adsorption–desorption isotherms of the sodium bentonite and aluminum pillared bentonite, which resemble an isotherm type IV from the Brunauer–Emmett–Teller (BET) classification. The BET specific surface area value of the raw bentonite is 77.23 m^2/g, and after the pillaring process, the specific surface area increases to the value of 169.051 m^2/g. The Brunauer–Deming–Deming–Teller (BDDT) classification methodology categorizes the nitrogen adsorption–desorption isotherms for the bentonite studied into the H4 hysteresis from the International Union of Pure and Applied Chemistry (IUPAC), typical for porous materials which contain mesoporous materials [45–47].

The pore size of sodium bentonite and aluminum pillared bentonite was determined by Barrett–Joyner–Halenda (BJH) method (Figure 6).

3.2.3. Energy Dispersive X-Ray (EDX) Coupled with Scanning Electron Microscopy

Energy Dispersion X-Ray (EDX) analysis was carried out concomitantly with SEM analysis for the raw material and aluminum pillared bentonite. Through this technique, the elemental composition of bentonite was identified at two certain points of interest, and the results are shown in Table 2.

From this elemental microanalysis presented in the previous paragraph, the results show changes to the mass level (wt. %) of the compounds after the pillaring process, with aluminum polyhydroxocations and the graphic representation presented in Figure 7.

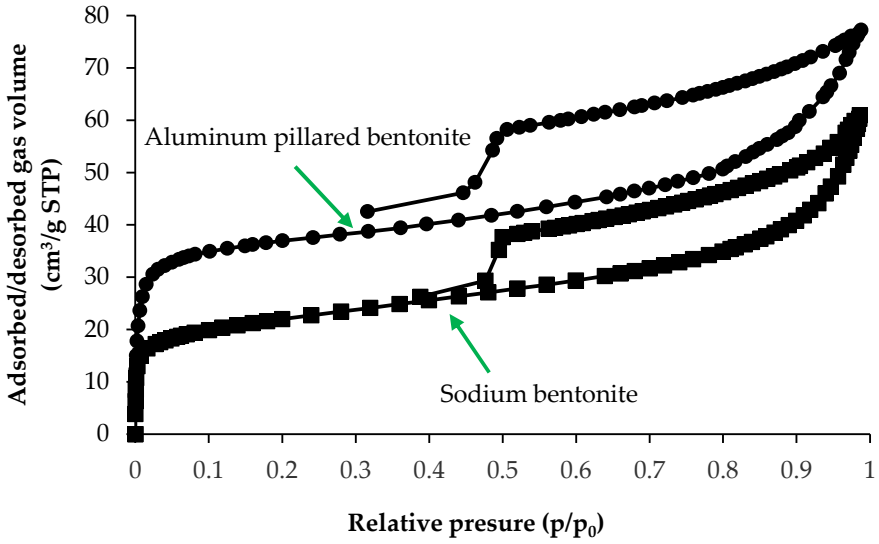


Figure 5. Nitrogen adsorption–desorption isotherms of the adsorbents.

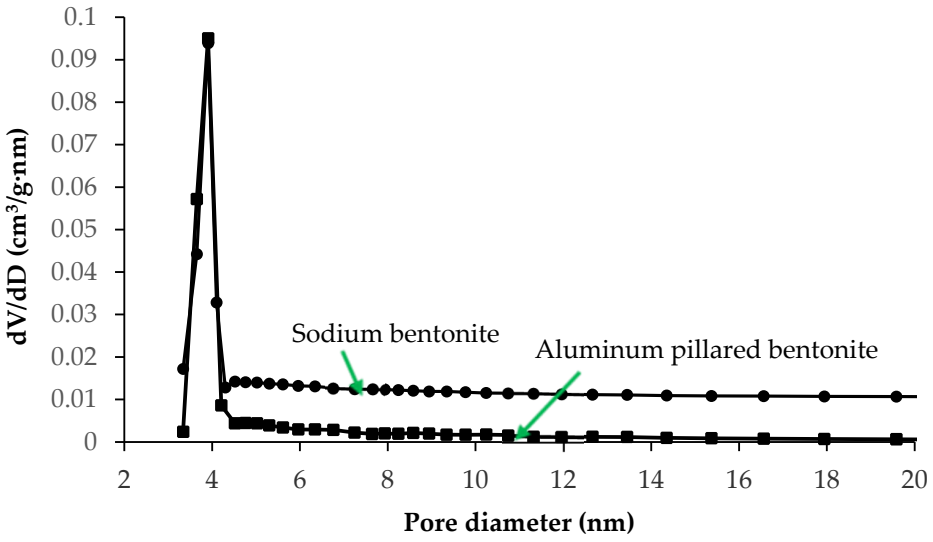


Figure 6. Pore size distributions of the adsorbents.

Table 2. Elemental microanalysis of adsorbents.

Chemical Element	Sodium Bentonite, (wt. %)	Aluminum Pillared Bentonite, (wt. %)
O	57.68	54.53
Na	2.45	0.18
Mg	1.92	1.75
Al	11.01	15.05
Si	26.22	27.69
K	0.08	0.07
Ca	0.08	0.07
Ti	0.05	0.10
Fe	0.52	0.54
Total	100.00	100.00

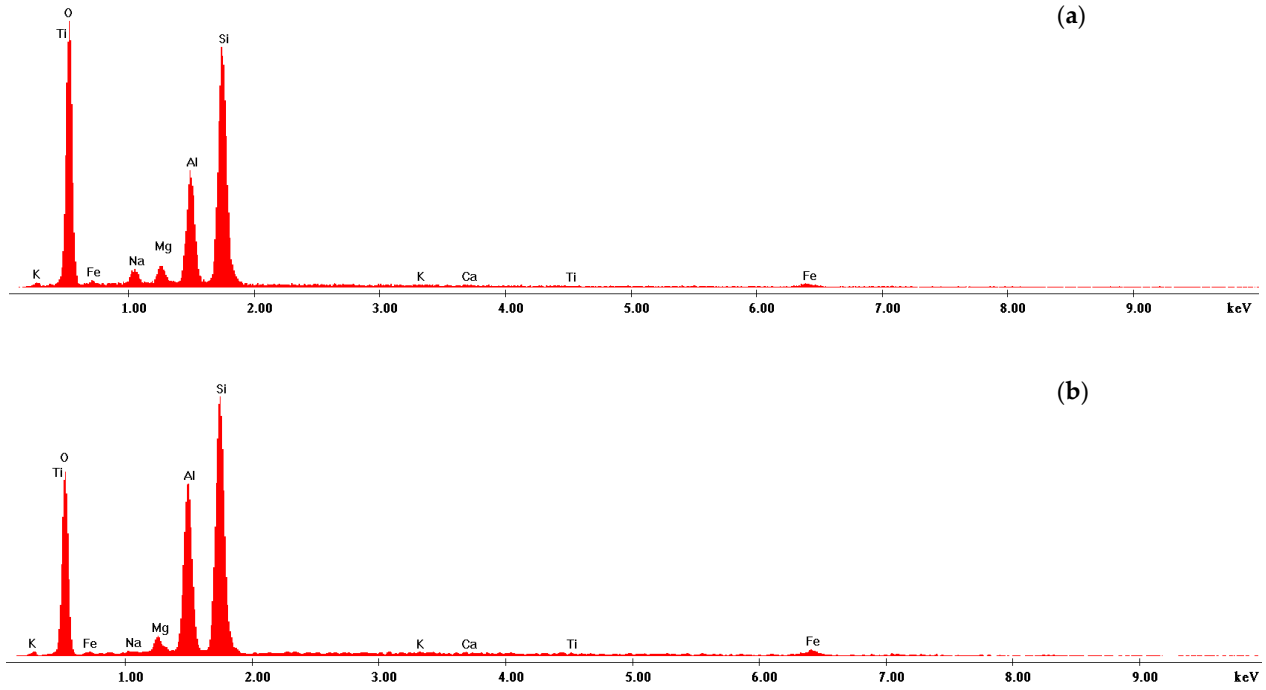
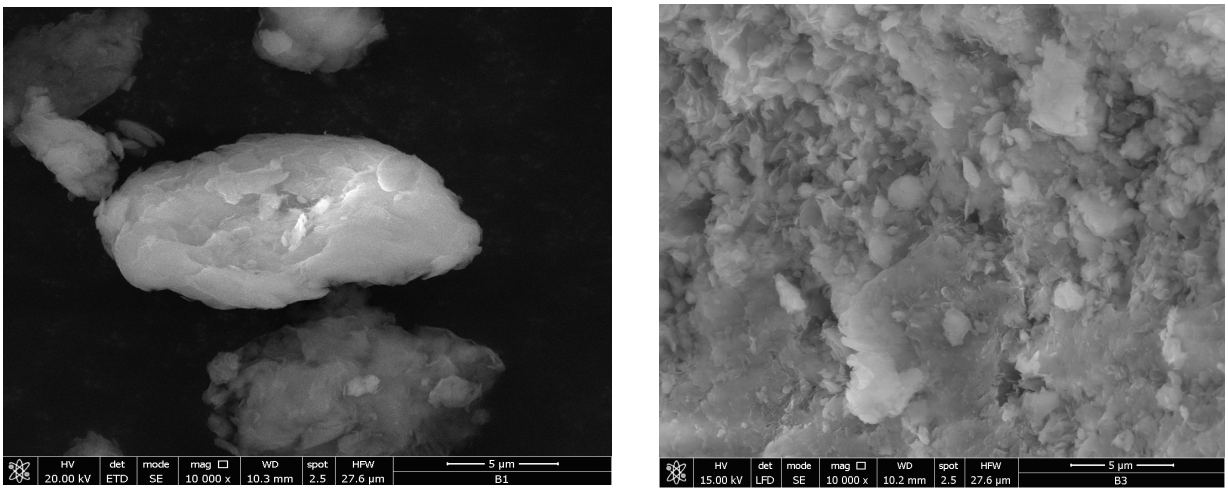


Figure 7. EDX analysis of (**a**) sodium bentonite; (**b**) aluminum pillared bentonite.

The masses of O, Na Mg, K, Ca forms of sodium bentonite decrease, because the introduction of aluminum cations in the structure of pillared bentonite causes the quantities of these elements to decrease. Conversely, the mass of Si and Al increases with the formation of the porous structure with rigid pillars of aluminum polyhydroxocations, which creates spaces for further molecule adsorption.

The SEM images of the sodium bentonite and of aluminum pillared bentonite are given in Figure 8.



(**a**) (**b**)

Figure 8. SEM images at 5 µm resolution of (**a**) sodium bentonite; (**b**) aluminum pillared bentonite.

Sodium bentonite has a homogenous structure, characteristic of the compounds known as the smectite family, with a 2:1 layer phyllosilicate, constituted generally by leaves, such as those mixed with large aggregates. In the case of aluminum pillared bentonite, it has a the appearance of a sponge structure, with smaller particles. In this material, the leaf-like structure has completely disappeared, and a more porous structure has been formed, in order to retain ammonia or carbon dioxide molecules.

3.3. Ammonia Adsorption

3.3.1. Experimental Matrix

Experimental investigations for ammonia adsorption on sodium bentonite and aluminum pillared bentonite depending on the gas–particle contact technique were performed using the experimental matrix reported in Table 3.

Table 3. Experimental matrix used in ammonia adsorption in fixed and fluidized bed.

No. Test	Adsorbent Particles	Average Particle Size ($\overline{d}_p$, μm)	Gas Velocity, (U_g, m/s)	Total Flow Rate, (Q_T, L/s)
1.	Sodium bentonite	750	$0.6 \times U_{mf}$	0.3341
2.			U_{mf}	0.5436
3.			$1.4 \times U_{mf}$	0.7525
4.		1500	$0.8 \times U_{mf}$	0.3341
5.			U_{mf}	1.34
6.			$1.2 \times U_{mf}$	2.3433
7.	Aluminum pillared bentonite	750	$0.6 \times U_{mf}$	0.3341
8.			U_{mf}	0.5436
9.			$1.4 \times U_{mf}$	0.7525
10.		1500	$0.8 \times U_{mf}$	0.3341
11.			U_{mf}	1.34
12.			$1.2 \times U_{mf}$	2.3433

3.3.2. Adsorption Kinetics

According to the dynamic particle studies from previous publications [46–55], the minimum fluidization velocity (U_{mf}) is considered to be equal to 0.27 m/s for the particle size $\overline{d}_p = 750$ μm, and the minimum fluidization velocity (U_{mf}) is equal to 0.67 m/s for the particle size $\overline{d}_p = 1500$ μm, in order to highlight the influence of the gas velocity formed from ammonia and air.

The first ammonia absorption took place in a fixed bed ($U_g = 0.6 \times U_{mf}$) and the following ammonia retentions in fluidized bed conditions, i.e., at the initial fluidization, when $U_g = U_{mf}$, and at the fluidization with small bubble gas, when $U_g = 1.4 \times U_{mf}$. The ammonia adsorption capacity on bentonite particles was measured until bed saturation, C/C_0~1.

Ammonia adsorption tests were performed on sodium bentonite particles previously prepared in small particles and characterized under different gas–particle contact conditions, as illustrated in Figure 9.

Analyzing the ammonia adsorption curves (Figure 9a), an increase in the adsorption capacity can be observed, recorded by the sodium bentonite particles, with the increase in the gas velocity (U_g) under the conditions mentioned above. At equilibrium, in the case of particle sizes with $\overline{d}_p = 750$ μm, the ammonia adsorption capacity varies at saturation from 0.326 mmol NH_3/g in a fixed bed to 0.436 mmol NH_3/g in incipient fluidization and to 0.553 mmol NH_3/g in a homogeneous fluidized bed. In a fixed bed, it can observe that the bed saturation occurs after 455 s, and in a fluidized state, the bed saturation occurs immediately, after 115 to 154 s.

A similar variation of the ammonia adsorption capacity occurs in the case of particle sizes with $\overline{d}_p = 1500$ μm (Figure 9b); in a fixed bed, the value is 0.357 mmol NH_3/g with bed saturation after 514 s. Under incipient fluidization ($U_g = U_{mf}$), the ammonia adsorption capacity is 0.518 mmol NH_3/g and particle bed is saturated after 150 s.

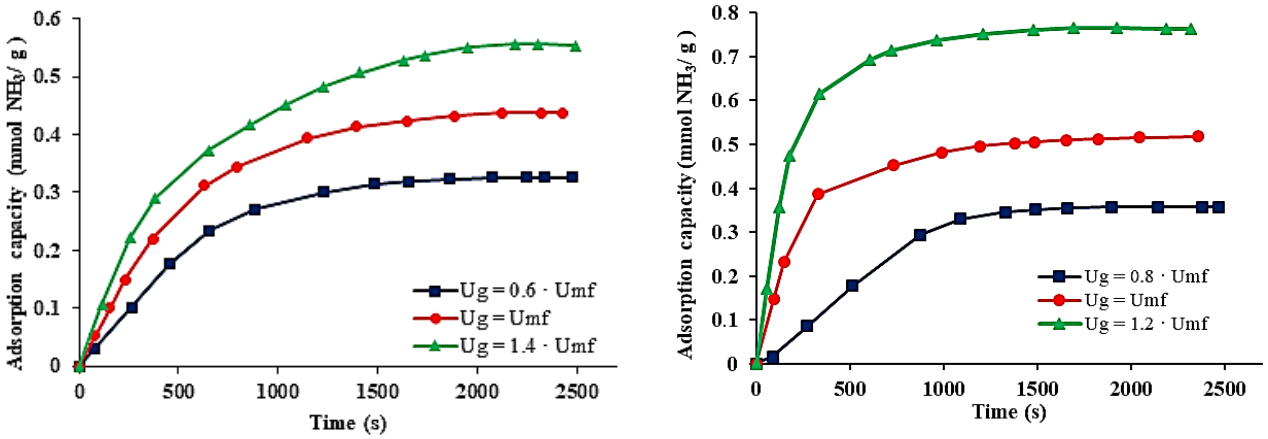


Figure 9. Ammonia adsorption kinetics on sodium bentonite particles with L_0/D = 2 and C_0 = 3800 ppm. (**a**) $\overline{d}_p$ = 750 µm; (**b**) $\overline{d}_p$ = 1500 µm.

In a homogeneous fluidization bed, when $U_g = 1.2 \times U_{mf}$, the ammonia adsorption capacity is 0.763 mmol NH_3/g and the bed saturation happens immediately, after 125 s.

The influence of ammonia adsorption capacity depending on the gas–particle contact technique for aluminum bentonite particles is shown in Figure 10.

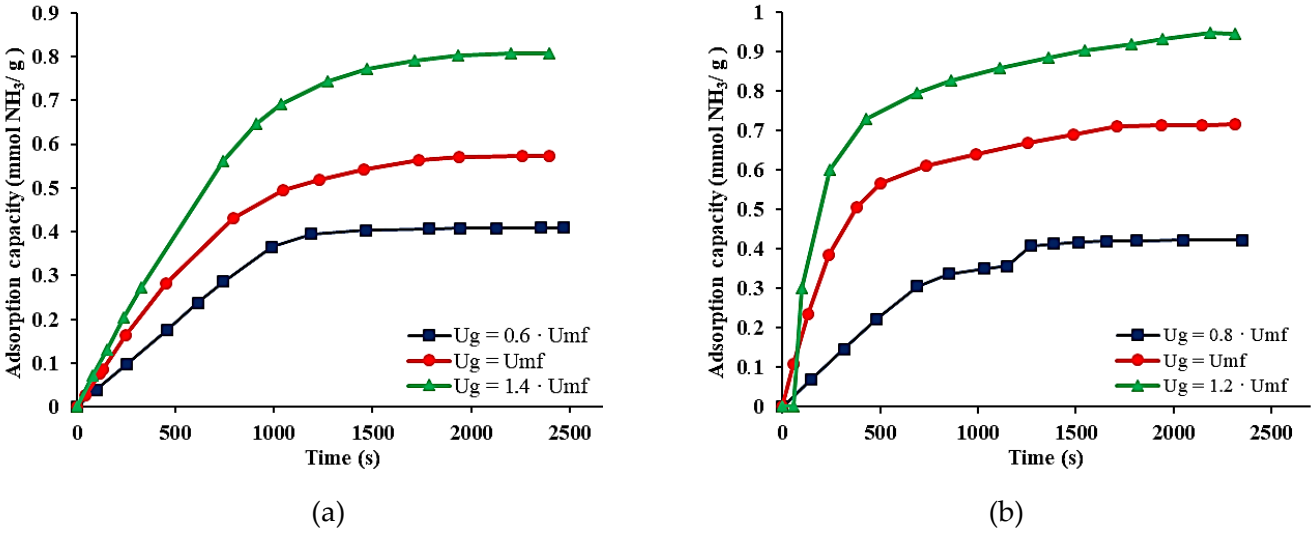


Figure 10. Ammonia adsorption kinetics on aluminum pillared bentonite particles with L_0/D = 2 and C_0 = 3800 ppm. (**a**) $\overline{d}_p$ = 750 µm; (**b**) $\overline{d}_p$ = 1500 µm.

The kinetic curve shows that the particles with $\overline{d}_p$ = 750 µm (Figure 10a) exhibit, in the fixed bed, a lower value of ammonia adsorption capacity of 0.409 mmol NH_3/g at bed saturation after 742 s. In the case of incipient fluidization, the ammonia adsorption capacity is 0.572 mmol NH_3/g and the particle bed saturation occurs after 245 s. When $U_g = 1.4 \times U_{mf}$, the ammonia adsorption capacity registered is 0.804 mmol NH_3/g and the bed saturation happens after 235 s.

The aluminum bentonite particles with $\overline{d}_p$ = 1500 µm (Figure 10b) exhibited the highest values for ammonia adsorption capacity at saturation. The best ammonia adsorption capacity in the fixed bed is 0.421 mmol NH_3/g with bed saturation after 482 s. The estimated ammonia adsorption capacity of aluminum pillared particles in the fluidized bed is under incipient fluidization to 0.716 mmol NH_3/g with particle bed saturation after 130 s

and under homogeneous fluidization with ammonia adsorption capacity of 0.945 mmol NH_3/g and particle bed saturation after 100 s.

3.4. Desorption and Regeneration Studies

In order to recover the bentonite particles with $\overline{d}_p = 1500$ μm, the ammonia desorption and adsorbent regeneration processes were also studied in a fixed bed. Ammonia desorption experiments were performed by thermo-desorption technique in the presence of nitrogen. The installation is presented in Figure 1.

The calculation of the desorption capacity and desorption efficiency (%) was carried out taking as a reference the first value recorded at the first thermo-desorption. The approximate values of the four cycles of regeneration for ammonia by thermo-desorption are presented in Table 4.

Table 4. Values of ammonia desorption capacity and desorption efficiency (%).

No. of Cycles	Sodium Bentonite Particles		Aluminum Pillared Bentonite Particles	
	mmol NH_3 Desorbed/g Bentonite	%	mmol NH_3 Desorbed/g Bentonite	%
0.	0.357	100	0.527	100
1.	0.245	68.62	0.464	95.44
2.	0.158	44.25	0.345	88.04
3.	0.062	17.36	0.268	50.85
4.	-	0.00	0.088	16.69

After ammonia gas saturation and thermal treatment of the adsorbent particles, it was observed that the ammonia desorbed capacity from the bentonite decreases with the number of regeneration cycles. The sodium bentonite particles lose less than half of their capacity (44.25%) after two cycles. In the case of aluminum pillared bentonite, the loss is 50.85% after four cycles.

This phenomenon is absolutely normal because there are structural changes at the level of specific surface area and basal spacing, being a rigid material. Both adsorbents can be regenerated at least three times without losing their initial properties.

They can be considered good materials for industrial-level applications with low consumption of effort and energy.

4. Conclusions

In this study, sodium bentonite was modified by a pillaring process with aluminum polyhydroxocations to improve adsorption performance for ammonia from air.

The measurements carried out on the sodium bentonite showed that this type of clay can be subjected to the ammonia adsorption process because it can be agglomerated to form adsorbent particles. This material presents an acid–base character and the measurements showed the existence of acidic sites having high surface acidity values, being able to retain some molecules like ammonia.

Surface chemical characterization results showed that the modification by pillaring led to an increase in basal spacing, specific surface area, pore volume and pore diameter of aluminum pillared bentonite, improving ammonia adsorption capacity.

The ammonia adsorption kinetics were measured on sodium bentonite and on aluminum pillared bentonite with different gas–particle contact methods, and the ammonia adsorption capacity was calculated.

Therefore, under fluidized bed conditions, sodium bentonite and aluminum pillared bentonite particles exhibited superior adsorption capacity compared to a fixed bed. In a

fluidized bed, the mass transfer zone of the bed particles is higher due to the dynamic conditions by increasing the ammonia–particle surface contact. In these conditions, the aluminum pillared bentonite particle bed is saturated very quickly after 100 s and the optimal value recorded for ammonia adsorption capacity is 0.945 mmol NH_3/g.

The ammonia adsorption performance is very good for the bentonite pillared with aluminum polyhydroxocations and presents advantages of a simple pillaring process with low cost of preparation, which has very great application in air depollution.

Author Contributions: Conceptualization, G.M. and A.-M.G.; methodology, G.M.; software, C.V.J.; validation, G.M.; formal analysis, N.P. and V.A.A.; investigation, N.P. and V.A.A.; resources, I.D.N.; data curation, G.M. and A.-M.G.; writing—original draft preparation, A.-M.G. and A.-M.R.; writing—review and editing, G.M. and A.-M.R.; visualization, I.D.N.; supervision, C.V.J. and I.D.N.; project administration, I.D.N.; funding acquisition, A.-M.R. and I.D.N. All authors have read and agreed to the published version of the manuscript.

Funding: This research received no external funding.

Institutional Review Board Statement: Not applicable.

Informed Consent Statement: Not applicable.

Data Availability Statement: The original contributions presented in this study are included in the article. Further inquiries can be directed to the corresponding authors.

Acknowledgments: The authors are grateful to Gholamreza Djelveh and the entire team from Clermont University (ENSCCF), GePEB axis, for the technical support in carrying out the kinetics experiments.

Conflicts of Interest: The authors declare no conflicts of interest.

References

1. Venaruzzo, J.L.; Volzone, C.; Rueda, M.L.; Ortiga, J. Modified bentonitic clay minerals as adsorbents of CO, CO_2 and SO_2 gases. *Microporous Mesoporous Mater.* **2002**, *56*, 73–80. [CrossRef]
2. Vo, H.T.; Kim, J.; Kim, N.Y.; Lee, J.-K.; Joo, J.B. Effect of pore texture property of mesoporous alumina on adsorption performance of ammonia gas. *J. Ind. Eng. Chem.* **2020**, *91*, 129–138. [CrossRef]
3. Brodny, J.; Tutak, M. The analysis of similarities between the European Union countries in terms of the level and structure of the emissions of selected gases and air pollutants into the atmosphere. *J. Clean. Prod.* **2021**, *279*, 123641. [CrossRef] [PubMed]
4. Liu, Z.J.; Clay, S.A.; Clay, D.E.; Harper, S.S. Ammonia fertilizer influences atrazine adsorption-desorption characteristics. *J. Agric. Food Chem.* **1995**, *43*, 815–819. [CrossRef]
5. Guo, J.; Yang, H.; Yuan, Y.; Yin, P.; Zhang, N.; Lin, Z.; Ma, Q.; Yang, Q.; Liu, X.; Wang, H.; et al. Blending of Slow-Release N Fertilizer and Urea Improve Rainfed Maize Yield and Nitrogen Use Efficiency While Reducing Apparent N Losses. *Agronomy* **2025**, *15*, 11. [CrossRef]
6. Wyer, K.E.; Kelleghan, D.B.; Blanes-Vidal, V.; Schauberger, G.; Curran, T.P. Ammonia emissions from agriculture and their contribution to fine particulate matter: A review of implications for human health. *J. Environ. Manag.* **2022**, *323*, 116285. [CrossRef]
7. Busca, G.; Pistarino, C. Abatement of ammonia and amines from waste gases: A summary. *J. Loss Prevent. Process Ind.* **2003**, *16*, 157–163. [CrossRef]
8. Behera, S.N.; Sharma, M.; Aneja, V.P.; Balasubramanian, R. Ammonia in the atmosphere: A review on emission sources, atmospheric chemistry and deposition on terrestrial bodies. *Environ. Sci. Pollut. Res.* **2013**, *20*, 8092–8131. [CrossRef]
9. Mofidi, A.; Asilian, H.; Jafari, A.J. Adsorption of volatile organic compounds on fluidized activated carbon bed. *Health Scope* **2013**, *2*, 84–89. [CrossRef]
10. Han, B.; Butterly, C.; Zhang, W.; He, J.-Z.; Chen, D. Adsorbent materials for ammonium and ammonia removal: A review. *J. Clean. Prod.* **2021**, *283*, 124611. [CrossRef]
11. Zhu, R.; Chen, Q.; Zhou, Q.; Xi, Y.; Zhu, J.; He, H. Adsorbents based on montmorillonite for contaminant removal from water: A review. *Appl. Clay Sci.* **2016**, *123*, 239–258. [CrossRef]
12. Adeyemo, A.A.; Adeoye, I.O.; Bello, S.O. Adsorption of dyes using different types of clay: A review. *App. Water Sci.* **2017**, *7*, 543–568. [CrossRef]
13. Volzone, C. Retention of pollutant gases: Comparison between clay minerals and their modified products. *Appl. Clay Sci.* **2007**, *36*, 191–196. [CrossRef]

14. Erdoğan, B.; Ergürha, O.; Ante, A. Influence of acid activation on the NH_3-adsorption properties of a Turkish bentonite. *Clay Miner.* **2021**, *56*, 178–184. [CrossRef]
15. Konta, J. Clay and Man: Clay Raw Materials in the Service of Man. *Appl. Clay Sci.* **1995**, *10*, 275–335. [CrossRef]
16. Carriazo, J.G.; Saavedra, M.J.; Molina, M.F. XRD study on the intercalation-pillaring of a 2:1 clay mineral with aluminum polyoxocationic species. *Rev. Mex. Ing. Quim.* **2009**, *8*, 299–305.
17. Worasith, N.; Goodman, B.A. Clay mineral products for improving environmental quality. *Appl. Clay Sci.* **2023**, *242*, 106980. [CrossRef]
18. Ursu, A.V.; Gros, F.; Nistor, D.I.; Djelveh, G. Characterization and utilization of a commercial clay for ammonia adsorption: Influence of operating parameters on gas retaining. *Rev. Chim.* **2008**, *59*, 1067–1072. [CrossRef]
19. Platon, N.; Siminiceanu, I.; Nistor, I.D.; Miron, N.D.; Muntianu, G.; Mares, A.M. Fe—Pillared clay as an efficient Fenton-like heterogeneous catalyst for phenol degradation. *Rev. Chim.* **2011**, *62*, 676–679.
20. Ding, Z.; Kloprogge, J.T.; Frost, R.L. Porous clays and pillared clays-based catalysts. Part 2: A review of the catalytic and molecular sieve applications. *J. Porous Mater.* **2001**, *8*, 273–293. [CrossRef]
21. Hortolomeu, A.; Mirila, D.C.; Roșu, A.-M.; Nedeff, F.M.; Scutaru, I.; Ureche, D.; Sturza, R.; Fînaru, A.-L.; Nistor, I.D. Chemically Modified Clay Adsorbents Used in the Retention of Protein and Polyphenolic Compounds from Sauvignon Blanc White Wine. *Nanomaterials* **2024**, *14*, 588. [CrossRef] [PubMed]
22. Maes, N.; Heylen, I.; Cool, P.; Vansant, E.F. The relation between the synthesis of pillared clays and their resulting porosity. *Appl. Clay Sci.* **1997**, *12*, 43–60. [CrossRef]
23. Muthu, M.; Sadowski, Ł. Evaluation of the Performance of Pervious Concrete Inspired by CO2-Curing Technology. *Appl. Sci.* **2024**, *14*, 4202. [CrossRef]
24. Li, M.; Zhang, X.; Su, W.; Cai, F.; Lan, T.; Dai, Z. Adsorption of Coxsackievirus in Sediments: Influencing Factors, Kinetics, and Isotherm Modeling. *Appl. Sci.* **2024**, *14*, 1480. [CrossRef]
25. Ouakouak, A.; Abdelhamid, M.; Thouraya, B.; Chahinez, H.-O.; Hocine, G.; Hamdi, N.; Syafiuddin, A.; Boopathy, R. Development of a Novel Adsorbent Prepared from Dredging Sediment for Effective Removal of Dye in Aqueous Solutions. *Appl. Sci.* **2021**, *11*, 10722. [CrossRef]
26. Kurian, M.; Sugunan, S. Characterisation of the acid-base properties of pillared montmorillonites. *Microporous Mesoporous Mater.* **2005**, *83*, 25–34. [CrossRef]
27. Shin, Y.S.; Geun, S.; Ha, B.H. Pore structures and acidities of Al-pillared montmorillonite. *Korean J. Chem. Eng.* **2003**, *20*, 77–82. [CrossRef]
28. Rodríguez-González, L.; Rodríguez-Castellón, E.; Jiménez-López, A.; Simon, U. Correlation of TPD and impedance measurements on the desorption of NH_3 from zeolite H-ZSM-5. *Solid State Ion.* **2008**, *179*, 1968–1973. [CrossRef]
29. Sakr, A.K.; Cheira, M.F.; Hassanin, M.A.; Mira, H.I.; Mohamed, S.A.; Khandaker, M.U.; Osman, H.; Eed, E.M.; Sayyed, M.I.; Hanfi, M.Y. Adsorption of Yttrium Ions on 3-Amino-5-Hydroxypyrazole Impregnated Bleaching Clay, a Novel Sorbent Material. *Appl. Sci.* **2021**, *11*, 10320. [CrossRef]
30. Stanly, S.; Jelmy, E.J.; Nair, C.P.R.; John, H. Carbon dioxide adsorption studies on modified montmorillonite clay/reduced graphene oxide hybrids at low pressure. *J. Environ. Chem. Eng.* **2019**, *7*, 103344. [CrossRef]
31. Azzouz, A.; Nistor, D.; Miron, D.; Ursu, A.V.; Sajin, T.; Monette, F.; Niquette, P.; Hausler, R. Assessment of acid-base strength distribution of ion-exchanged montmorillonites through NH_3 and CO_2-TPD measurements. *Thermochim. Acta* **2006**, *449*, 27–34. [CrossRef]
32. Ayari, F.; Srasra, E.; Trabelsi-Ayadi, M. Characterization of bentonitic clays and their use as adsorbent. *Desalination* **2005**, *185*, 391–397. [CrossRef]
33. De Stefanis, A.; Tomlinson, A.A.G. Towards designing pillared clays for catalysis. *Catal. Today* **2006**, *114*, 126–141. [CrossRef]
34. Altunlu, M.; Yapar, S. Effect of OH-/Al3+ and Al3+/clay ratios on the adsorption properties of Al-pillared bentonites. *Colloids Surf. A Physicochem. Eng. Asp.* **2007**, *306*, 88–94. [CrossRef]
35. Cool, P.; Vansant, E.F. Pillared Clays: Preparation, Characterization and Applications. In *Synthesis*; Part of the Molecular Sieves Book Series (SIEVES, volume 1); Springer: Berlin/Heidelberg, Germany, 2001.
36. Salerno, P.; Mendioroz, S. Preparation of Al-pillared montmorillonite from concentrated dispersions. *Appl. Clay Sci.* **2002**, *22*, 115–123. [CrossRef]
37. Georgescu, A.M.; Platon, N.; Arus, V.A.; Jinescu, C.; Nardou, F.; Nistor, I.D. Study on the preparation and characterization of aluminum-pillared clays using montmorillonite K10. *Sci. Study Res.-Chem. Chem. Eng. Biotechnol. Food Ind.* **2023**, *24*, 145–153.
38. Khanh, T.S.T.; Trung, T.Q.; Giang, L.T.T.; Nguyen, T.Q.; Lam, N.D.; Dinh, N.N. Ammonia Gas Sensing Characteristic of P3HT-rGO-MWCNT Composite Films. *Appl. Sci.* **2021**, *11*, 6675. [CrossRef]
39. Muntianu, G.; Georgescu, A.M.; Nistor, I.D.; Jinescu, G. Ammonia adsorption kinetics on clay particles in fluidized bed. *Bull. Rom. Chem. Eng. Soc.* **2016**, *3*, 2–11.

40. Al-Ghurabi, E.H.; Ajbar, A.; Asif, M. Improving Fluidization Hydrodynamics of Group C Particles by Mixing with Group B Particles. *Appl. Sci.* **2018**, *8*, 1469. [CrossRef]
41. Usuda, H.; Mishima, Y.; Kawamoto, T.; Minami, K. Desorption of Ammonia Adsorbed on Prussian Blue Analogs by Washing with Saturated Ammonium Hydrogen Carbonate Solution. *Molecules* **2022**, *27*, 8840. [CrossRef]
42. Ganachari, S.V.; Shilar, F.A.; Patil, V.B.; Khan, T.M.Y.; Saleel, C.A.; Ali, M.A. Optimizing Ammonia Detection with a Polyaniline−Magnesia Nano Composite. *Polymers* **2024**, *16*, 2892. [CrossRef] [PubMed]
43. Apostolov, A.; Panyovska, S.; Stefanov, S.; Dzhonova-Atanasova, D.; Razkazova-Velkova, E.; Michev, S. Integrated Absorption–Adsorption Process for Waste-Free Decontamination of Gases from Sulfur Dioxide, Part 2: CFD Modeling and Experimental Investigation of a Bubble-Cap Tray. *Sustainability* **2024**, *16*, 2472. [CrossRef]
44. Murtaza, M.; Ahmad, H.M.; Kamal, M.S.; Hussain, S.M.S.; Mahmoud, M.; Patil, S. Evaluation of Clay Hydration and Swelling Inhibition Using Quaternary Ammonium Dicationic Surfactant with Phenyl Linker. *Molecules* **2020**, *25*, 4333. [CrossRef]
45. Muntianu, G.; Platon, N.; Mardaru, A.; Nistor, I.D.; Miron, N.D.; Jinescu, G. Use of modified clays obtained by pillaring in gas purification. *Univ. Politeh. Buchar. Sci. Bull. Ser. B—Chem. Mater. Sci.* **2015**, *77*, 151–164.
46. Mugge, J.; Bosch, H.; Reith, T. Measuring and modelling gas adsorption kinetics in single porous particles. *Chem. Eng. Sci.* **2001**, *56*, 5351–5360. [CrossRef]
47. Castillo-Araiza, C.O.; Che-Galicia, G.; Dutta, A.; González, G.G.; Martínez-Vera, C.; Ruíz-Martínez, R.S. Effect of diffusion on the conceptual design of a fixed-bed adsorber. *Fuel* **2015**, *149*, 100–108. [CrossRef]
48. Manohar, D.M.; Noeline, B.F.; Anirudhan, T.S. Adsorption performance of Al-pillared bentonite clay for the removal of cobalt(II) from aqueous phase. *App. Clay Sci.* **2006**, *31*, 194–206. [CrossRef]
49. Ursu, A.V.; Jinescu, C.; Nistor, D.I.; Arus, V.A.; Isopencu, G.; Mares, A.M. Estimation of the Dynamic Parameters of Mono and Bicomponent Granular Particles Beds Fluidization. *Rev. Chim.* **2010**, *61*, 1226–1230.
50. Mirila, D.C.; Pirva, M.S.; Rosu, A.M.; Zichil, V.; Nistor, I.D. Activated adsorption on clay of micropollutants from paper printing industry. *Sci. Stud. Res. Chem.* **2018**, *19*, 63–72.
51. Rodrigues, C.C.; de Moraes, D., Jr.; da Nóbrega, S.W.; Barboza, M.G. Ammonia adsorption in a fixed bed of activated carbon. *Bioresour. Technol.* **2007**, *98*, 886–891. [CrossRef]
52. Muntianu, G.; Simion, A.-I.; Grigoraș, C.-G.; Platon, N.; Nistor, I.-D.; Jinescu, G. Aluminum pillared bentonite—Characterization and synthesis optimization by response surface methodology. *Stud. UBB Chem. LXVI* **2021**, *1*, 73–88. [CrossRef]
53. El Miz, M.; Salhi, S.; Chraibi, I.; El Bachiri, A.; Fauconnier, M.-L.; Tahani, A. Characterization and Adsorption Study of Thymol on Pillared Bentonite. *Open J. Phys. Chem.* **2014**, *4*, 98–116. [CrossRef]
54. Muntianu, G.; Platon, N.; Arus VA Rosu, A.M.; Nistor, D.I.; Jinescu, G. Hydrodynamic study of clay particles in fluidized bed. *J. Eng. Stud. Res.* **2013**, *19*, 70–75.
55. Muntianu, G.; Ursu, A.-V.; Djelveh, G.; Isopencu, G.; Mareș, A.-M.; Nistor, I.D.; Jinescu, C.V. Dynamic parameters for mixtures of pillared clay-magnetic particles in fluidized bed in coaxial magnetic field. *Rev. Chim.* **2014**, *65*, 1077–1085.

Disclaimer/Publisher's Note: The statements, opinions and data contained in all publications are solely those of the individual author(s) and contributor(s) and not of MDPI and/or the editor(s). MDPI and/or the editor(s) disclaim responsibility for any injury to people or property resulting from any ideas, methods, instructions or products referred to in the content.